Inorganic Chemistry

pubs.acs.org/IC Article

# Odd−Even Effect on the Spin-Crossover Temperature in Iron(II) Complex Series Involving an Alkylated or Acyloxylated Tripodal Ligand

Atsushi Kashiro, Wakana Kohno, and Takayuki Ishida*

Cite This: https://dx.doi.org/10.1021/acs.inorgchem.0c01296 Read Online

ACCESS | Metrics & More | Article Recommendations | Supporting Information

**ABSTRACT:** In the context of magneto-structural study, a relatively short alkyl group was introduced to anionic spin-crossover (SCO) building blocks based on $[Fe(py_3CR)(NCS)_3]^-$, where $py_3CR$ stands for tris(2-pyridyl)methyl derivatives. The linear alkyl and acyloxyl derivatives of $Me_4N[Fe(py_3CR)(NCS)_3]$ with R = $C_nH_{2n+1}$ ($n$ = 1−7) and $C_nH_{2n+1}CO_2$ ($n$ = 1−6) were synthesized, and the magnetic study revealed that all the compounds investigated here exhibited SCO. The SCO temperature ($T_{1/2}$) varied in 289−338 K for the alkylated compounds, and those of the acyloxylated ones were lower with a narrower variation width ($T_{1/2}$ = 216−226 K). The crystal structures of the former with $n$ = 3, 4, and 5 and the latter with $n$ = 1, 4, 5, and 6 were determined, and various molecular arrangements were characterized. There is no structural evidence for a molecular fastener effect. The plots on $T_{1/2}$ against $n$ displayed a pronounced odd−even effect; the SCO temperatures of the homologues with even $n$ are relatively higher than those of the homologues with odd $n$. The odd−even effect on $T_{1/2}$ may be related with the entropy difference across the SCO, rather than crystal field modification or intermolecular interaction. The present work will help molecular design to fine-tune $T_{1/2}$ by means of simple chemical modification like alkylation and acyloxylation.

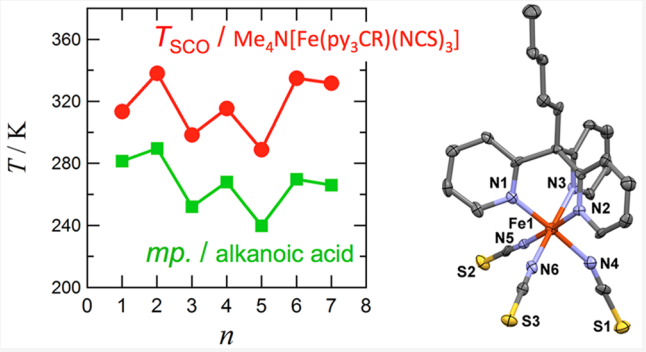




## INTRODUCTION

Various solid-state magnetic switches are attracting much attention to materials chemists because of future application to sensors, displays, memories, and other devices.[1,2] Spin crossover (SCO) materials involving an iron(II) high-spin (HS)/low-spin (LS) transition are the most intensively studied because alteration between paramagnetic ($S$ = 2) and diamagnetic ($S$ = 0) states would bring about a distinct switch of magnetic and/or chromic properties.

In such development stages, prediction, control, and fine-tuning of the SCO-related phenomena seem to be important issues, and the SCO is supposed to be regulated with a crystal field around the iron(II) ion on the basis of the molecular/crystal design.[3,4] In particular, the electron-donating/-withdrawing and steric substituent effects have much relation with the SCO behavior.[5] The SCO temperature can also be modulated by intermolecular interaction.[6] Introduction of moderate intermolecular interactions, such as $\pi-\pi$ stacking, hydrogen bonding, and hydrophobic interchain interactions, has been a beneficial challenge in crystal design toward multifunctional materials chemistry.[6,7] Long alkyl chains are often introduced to SCO materials as a mesogen in connection with possible cooperativity and bistability as well as trapping effects.[7,8] Actually, there have been several reports on the development of SCO liquid crystals and the application to soft matter.[9]

In the present study, however, a comparably short alkyl group was introduced to SCO building blocks in the context of the magneto-structural study. The motivation of the present study is to bestow the SCO materials an odd−even or parity effect. Various odd−even effects with respect to the carbon atom number in linear alkyl chains appear in many aspects. Typically, the alkanoic acids are well-known to display the odd−even alternation in their melting points; those with even-numbered carbon atoms in the alkyl portion are higher than the average of those of the nearest homologues with odd-numbered carbon atoms.[10] Interestingly, the reversal odd−even effect is often recorded; for example, dialkyl succinates with odd numbers of the carbon atoms in the alkyl side chain show higher melting points than the immediately adjacent analogues with even numbers.[11a] Breaking the odd−even

Received: May 1, 2020




https://dx.doi.org/10.1021/acs.inorgchem.0c01296
Inorg. Chem. XXXX, XXX, XXX−XXX

alternation has been reported for the self-assembly of linear bis(benzamides).[11b] The odd−even effects on the mesophase transition temperature have been studied for some liquid crystalline materials having a linear alkyl bridge.[12] The alkyl-substituted tetracenes are yellow to red in their solid state, depending on the parity of the atom number of the alkyl carbon atoms.[13a] Aggregation-induced emissive materials also exhibited an odd−even effect in chiral assembly.[13b] Furthermore, the odd−even behavior affects the molecular assembly and macroscopic crystal morphology.[14] A number of surface and interfacial materials carrying alkyl chains have many odd−even phenomena in the structures and properties.[15] Assuming the trans zigzag conformation of the alkyl group in the isomorphous crystal lattice, the end chain interaction is alternating by an $sp^3$-hybridized angle, 109.5°, with an increase of the number of carbon atoms.[16]

Thermodynamic parameters exhibited an odd−even effect across phase transition phenomena.[10,11,17] The transition temperature is regulated by the relation $T_{tr} = \Delta_{tr}H/\Delta_{tr}S$. The odd−even effects are explained in terms of the crystal packing and alkyl conformation.[11−17] However, if $T_{tr}$ is elevated/lowered, one can hardly tell whether an origin resides in enhanced/reduced $\Delta_{tr}H$, reduced/enhanced $\Delta_{tr}S$, or both. A combined study from structural and thermodynamic experiments is required to obtain further insight into this question.

We have so far developed the SCO complexes using $[Fe(py_3CR)(NCS)_3]^-$ building blocks, where $py_3CR$ stands for tris(2-pyridyl)methyl derivatives with R = H, OH, $CH_3$, py, and so on (Scheme 1).[18] Anionic SCO complex ions are somewhat rare, and furthermore the $[Fe(py_3CR)(NCS)_3]^-$ family exhibits a range of interesting SCO properties; $Me_4N[Fe(py_3COH)(NCS)_3](H_2O)$ showed thermal hysteresis with a temperature-scan rate dependence,[18a] $[Fe(py_4C)_2][Fe(py_4C)(NCS)_3]_2$ exhibited efficient light-induced excited spin-state trapping,[18d] $Me_4N[Fe(py_3C\text{-}n\text{-}C_{18}H_{37})(NCS)_3]$ displayed an order−disorder structural transition accompanied by SCO,[18e] and the first $FeN_4S_2$ SCO compounds were discovered in dinuclear $[\{Fe(py_3COH)(NCS)(\mu\text{-}NCS)\}_2](PrOH)_2$[18f] and polynuclear derivatives.[19] In this study, on varying the length of the R portions (Scheme 1), we systematically investigated the SCO temperature depending on *n*, the number of carbon atoms in R.

**Scheme 1. Structural Formulas of $py_3CR$ (Left) and $py_3COC(O)R$ (Right)**

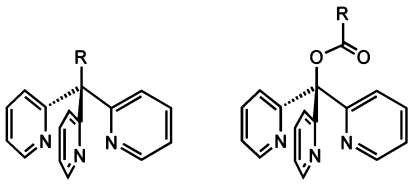


## MATERIALS AND METHODS

Derivatization of $py_3CR$ from 2-picoline has been established in the line of R = $CH_3$[20] and $C_{18}H_{37}$(stearyl).[18e] The tripodal alkylated ligands $py_3CC_nH_{2n+1}$ (*n* = 1−7) were thus prepared according to the established method. The key step is a double aromatic nucleophilic substitution of 2-halopyridine, and the yields were often low. Esterification on $py_3COH$ can be subjected to a manner for the known acetate $py_3COC(O)CH_3$.[21] The tripodal ester ligands $py_3COC(O)C_nH_{2n+1}$ (*n* = 1−6) were prepared in reasonable yields.

After the ligands, $py_3CR$ and $py_3COC(O)R$, were separated and purified, complex formation with iron(II) chloride, lithium thiocyanate, and tetramethylammonium chloride in methanol gave corresponding target complexes, $Me_4N[Fe(py_3CC_nH_{2n+1})(NCS)_3]$ (**1a**− **7a** for *n* = 1−7) and $Me_4N[Fe(py_3COC(O)C_nH_{2n+1})(NCS)_3]$ (**1e**− **6e** for *n* = 1−6) as light brown to red polycrystals. They turned dark red at 100 K. The molar ratio of the reactants was optimized for decreasing bis(tripod) complexes as a byproduct. The samples were subjected to elemental, spectroscopic, and magnetic analyses without further purification. The absence of solvent molecules was confirmed by means of elemental analysis and infrared spectroscopy. X-ray quality crystals were applied to the structural study.

X-ray diffraction data of a single crystal were collected on a RIGAKU Saturn70 CCD diffractometer with graphite monochromated Mo K$\alpha$ radiation ($\lambda$ = 0.71073 Å) at 100 K. Selected crystallographic data are given in Table 1. CCDC reference numbers 1993173, 1999658, 1993174, 1993175, 1993176, 1993177, and 1993179 are for **3a**, **4a**, **5a**, **1e**, **4e**, **5e**, and **6e**, respectively. For the ester compounds, the structures were also determined at 296 K. Selected crystallographic data are listed in Table S1 (Supporting Information). CCDC reference numbers 2006066, 2006067, 1993178, and 2006068 are for **1e**, **4e**, **5e**, and **6e**, respectively.

Magnetic susceptibilities of polycrystalline samples were measured on a Quantum Design MPMS-XL7 SQUID magnetometer with an applied field of 5000 Oe. No thermal hysteresis was recorded in repeated measurements on heating and cooling between 10 and 400 K. For details of the experiments, see the Supporting Information.

## RESULTS

**Crystal Structures.** Crystal structures have successfully been determined for **3a**, **4a**, **5a**, **1e**, **4e**, **5e**, and **6e** (Table 1), and the space groups are $P\bar{1}$, $P\bar{1}$, $P2_1/c$, $P2_1/c$, $P2_1/n$, $P\bar{1}$, and $P\bar{1}$, respectively. The molecular structures (except side chains) are quite similar to each other, as shown in Figure 1 (left panels). A tripodal *N*,*N*′,*N*″-tridentate donor, $py_3CR$, and three $NCS^-$ coligands afforded an $FeN_6$ coordination sphere. Although the Fe-$NCS^-$ portions were somewhat bent, the $[Fe(py_3CR)(NCS)_3]^-$ core possesses an approximate $C_{3v}$ symmetry. The Fe−N bond lengths in these compounds varied in ca. 1.92−1.99 Å at 100 K, being assignable to LS iron(II) ions. The countercation $Me_4N^+$ is usually found near the $NCS^-$ coligands, just like being embraced with three facial-configured $NCS^-$ groups (Figure S1, Supporting Information). We have to pay attention to the molecular arrangement in each crystal, especially folding patterns of alkyl side chains, as described below. Very interestingly, various packing motifs appeared (Figure 1, right panels).

As Table 1 and Figure 1a show, **3a** crystallizes in a triclinic $P\bar{1}$ space group. The propyl groups, having an anti conformation, are arranged in a layer structure parallel to the crystallographic *ac* plane, together with NCS ligands and $Me_4N$ ions. Two nearest-neighboring propyl groups are related with a crystallographic centrosymmetry and arranged in a head-to-head manner, not side-by-side. The interatomic distance between the alkyl terminal carbon atoms is 3.777(3) Å. No disorder was found, and the thermal displacement of every atom was considerably small at 100 K. Since the present series has an anionic charge at the iron(II) complex, we checked possible S···H−C interactions.[22] The shortest distances are 2.82 Å for S1···H14$^{i}$ and 2.94 Å for S1···H2$^{ii}$ (the symmetry operation codes of i and ii are $-x$, $-y+1$, $-z+1$ and $x$, $y+1$, $z$, respectively, being shorter than the sum of the van der Waals radii (S/H: 3.0 Å).[23] The contacting hydrogen atoms belong to pyridine rings in neighboring molecules, and this finding


https://dx.doi.org/10.1021/acs.inorgchem.0c01296
Inorg. Chem. XXXX, XXX, XXX−XXX

**Table 1. Selected Crystallographic Parameters of 3a, 4a, 5a, 1e, 3e, 4e, 5e, and 6e, Measured at 100 K**

| compound | 3a | 4a | 5a | 1e | 4e | 5e | 6e |
|---|---|---|---|---|---|---|---|
| formula | $C_{26}H_{31}FeN_7S_3$ | $C_{27}H_{33}FeN_7S_3$ | $C_{28}H_{35}FeN_7S_3$ | $C_{25}H_{27}FeN_7O_2S_3$ | $C_{28}H_{33}FeN_7O_2S_3$ | $C_{29}H_{35}FeN_7O_2S_3$ | $C_{30}H_{37}FeN_7O_2S_3$ |
| formula weight | 593.60 | 607.63 | 621.66 | 609.56 | 651.64 | 665.67 | 679.69 |
| crystal system | triclinic | triclinic | monoclinic | monoclinic | monoclinic | triclinic | triclinic |
| space group | $P\bar{1}$ | $P\bar{1}$[c] | $P2_1/c$ | $P2_1/c$ | $P2_1/n$ | $P\bar{1}$ | $P\bar{1}$ |
| $a$/Å | 9.2099(19) | 9.2611(18) | 9.1655(19) | 12.4158(18) | 8.321(4) | 9.107(2) | 9.180(3) |
| $b$/Å | 11.130(2) | 11.847(2) | 13.567(3) | 8.9043(11) | 27.133(11) | 11.962(3) | 12.000(4) |
| $c$/Å | 14.182(3) | 13.819(2) | 23.870(5) | 25.163(4) | 13.773(12) | 16.391(4) | 16.549(8) |
| $\alpha$/deg | 74.355(9) | 73.673(5) | 90. | 90. | 90. | 100.092(12) | 99.78(6) |
| $\beta$/deg | 87.917(10) | 90.063(6) | 91.223(9) | 94.402(6) | 90.921(7) | 105.352(12) | 105.90(5) |
| $\gamma$/deg | 85.449(10) | 89.848(6) | 90. | 90. | 90. | 106.713(11) | 105.91(5) |
| $V$/Å$^3$ | 1395.3(5) | 1455.0(5) | 2967.5(10) | 2773.7(7) | 3109(3) | 1586.9(7) | 1625.9(15) |
| $Z$ | 2 | 2 | 4 | 4 | 4 | 2 | 2 |
| $d_{calcd}$/g·cm$^{-3}$ | 1.413 | 1.387 | 1.391 | 1.460 | 1.392 | 1.393 | 1.388 |
| $\mu$ (MoK$\alpha$)/mm$^{-1}$ | 0.794 | 0.763 | 0.750 | 0.806 | 0.724 | 0.711 | 0.695 |
| no. of unique refls. | 24025 | 16770 | 46614 | 26141 | 34800 | 27796 | 27414 |
| $R(F)$ ($I > 2\sigma(I)$)[a] | 0.0327 | 0.1376 | 0.0380 | 0.0680 | 0.0524 | 0.0670 | 0.0592 |
| $wR(F^2)$ (all refls.)[b] | 0.0758 | 0.3477 | 0.0913 | 0.1238 | 0.0872 | 0.1889 | 0.1849 |
| GOF parameter | 1.042 | 1.475 | 1.036 | 1.037 | 1.279 | 1.113 | 1.103 |
| $\Delta\rho_{max}$, $\Delta\rho_{min}$/e Å$^{-3}$ | 0.32, −0.41 | 2.82, −1.05 | 0.52, −0.55 | 0.50, −0.56 | 0.33, −0.32 | 1.76, −0.95 | 1.16, −0.76 |

[a] $R = \Sigma[|F_0| - |F_c|]/\Sigma|F_0|$. [b] $wR = [\Sigma w(F_0^2 - F_c^2)/\Sigma wF_o^4]^{1/2}$. [c] The cell parameters are chosen as a nonstandard setting for the sake of comparison with those of **3a**.

suggests that the S···H−C interactions may play an important role in the arrangement of the complex anion portion.

The crystal determination of **4a** left relatively large final $R$ values, owing to a small size and possible twinning of crystals. This may be related to the presence of a directional disorder of the $[Fe(py_3CC_4H_9)(NCS)_3]^-$ portion: a reversal position between an iron(II) ion and a tris(2-pyridyl)methyl quaternary carbon atom. However, eventually the molecular structure and thermal displacement factors for the major atomic positions were reasonably refined without introduction of any disorder model (Figure 1b). The butyl group has an anti zigzag conformation, and the thermal displacement was relatively small. The crystal of **4a** is practically isomorphous to that of **3a**, as supported with the cell parameters (Table 1), regardless of the difference of the side chains. The interatomic distance between the alkyl terminal carbon atoms is 3.92(2) Å.

On the other hand, **5a** crystallizes in a monoclinic $P2_1/c$ (Figure 1c). The pentyl group displays an all-anti zigzag conformation. No disorder occurs throughout the alkyl group. The pentyl groups, NCS ligands, and $Me_4N$ ions are gathered together in a layer parallel to the $ab$ plane in the crystal of **5a**. The nearest pentyl groups, related with a centrosymmetry, are separated by >4.0 Å. In comparison with **3a** and **4a**, the crystal system and space group of **5a** are different; and accordingly intermolecular contacts are different, but a layered structure has been found in common. No appreciable van der Waals contact is observed with respect to the alkyl group for **3a**, **4a**, or **5a**.

Figure 1d shows the crystal structure of **1e** in a monoclinic $P2_1/c$ space group, and the acetyl group in **1e** is surrounded with a NCS ligand, pyridine ring, and acetyl group from neighboring molecules. Probably the acetyl methyl group is too short, so that they cannot penetrate into the ionic-like layer consisting of the NCS and $Me_4N$ ions. In other words, the acetyl methyl groups are well separated from each other.

The space group of the crystal of **4e** is monoclinic $P2_1/n$ (Figure 1e), which is a different cell setting of $P2_1/c$ but favorable because of a "more orthorhombic" unit cell. The cell can be converted to $P2_1/c$, giving $a$ = 13.773(12), $b$ = 27.133(11), $c$ = 15.976(10) Å, and $\beta$ = 148.62(2)°. Thus, despite the same space group of **1e** and **4e**, the molecular arrangements are completely different. It should be noted that the butyl group in **4e** showed a gauche conformation at the terminal methyl group. It may be caused by the intermolecular van der Waals repulsive interaction between the terminal methyl and an $NCS^-$ sulfur atom in a neighboring molecule. The butyl group penetrates the ionic layer, and the shortest intermolecular alkyl···alkyl distance is recorded between the terminal methyl carbon atoms (3.896(5) Å). The crystal packing seems to be rigid, as indicated with the small displacement factors and the absence of disorder.

Compound **5e** crystallizes in triclinic $P\bar{1}$. The pentyl group in **5e** showed a gauche conformation in the central C−C bond. Namely, the side chain structures of **4e** and **5e** are quite similar to each other except for an additional methyl in **5e**. Similarly, the gauche formation may be owing to intermolecular reasons: van der Waals repulsive interactions between the terminal ethyl moiety and a pyridine ring in a neighboring molecule. The two facing pentyl groups are related with a centrosymmetry. Relatively large thermal displacement factors can be found around the gauche-configured carbon atoms, suggesting the internal angular motion in the alkyl group. Whereas no disorder model is required in the pentyl group, a disorder model has been introduced to the $Me_4N$ ion. Resultant thermal displacement factors in the $Me_4N$ ions are still large. A loose packing motif seems to be located in a pentyl-$Me_4N$ layer, parallel to the crystallographic $b + c$ direction.

Figure 1g shows the crystal structure of **6e** in a triclinic $P\bar{1}$ space group. The hexyl chain has a severe disorder with the optimized major/minor ratio of 0.599(5)/0.401(5). As for the terminal methyl group in the major skeleton, the third disordered position was found with the occupancy factor of 0.313(7)/0.287(8). Only the skeleton with the largest occupancy is drawn in Figure 1g. The hexyl moieties from the neighboring molecules are faced to each other with a centrosymmetric relation. There are two gauche conformations


https://dx.doi.org/10.1021/acs.inorgchem.0c01296
Inorg. Chem. XXXX, XXX, XXX−XXX

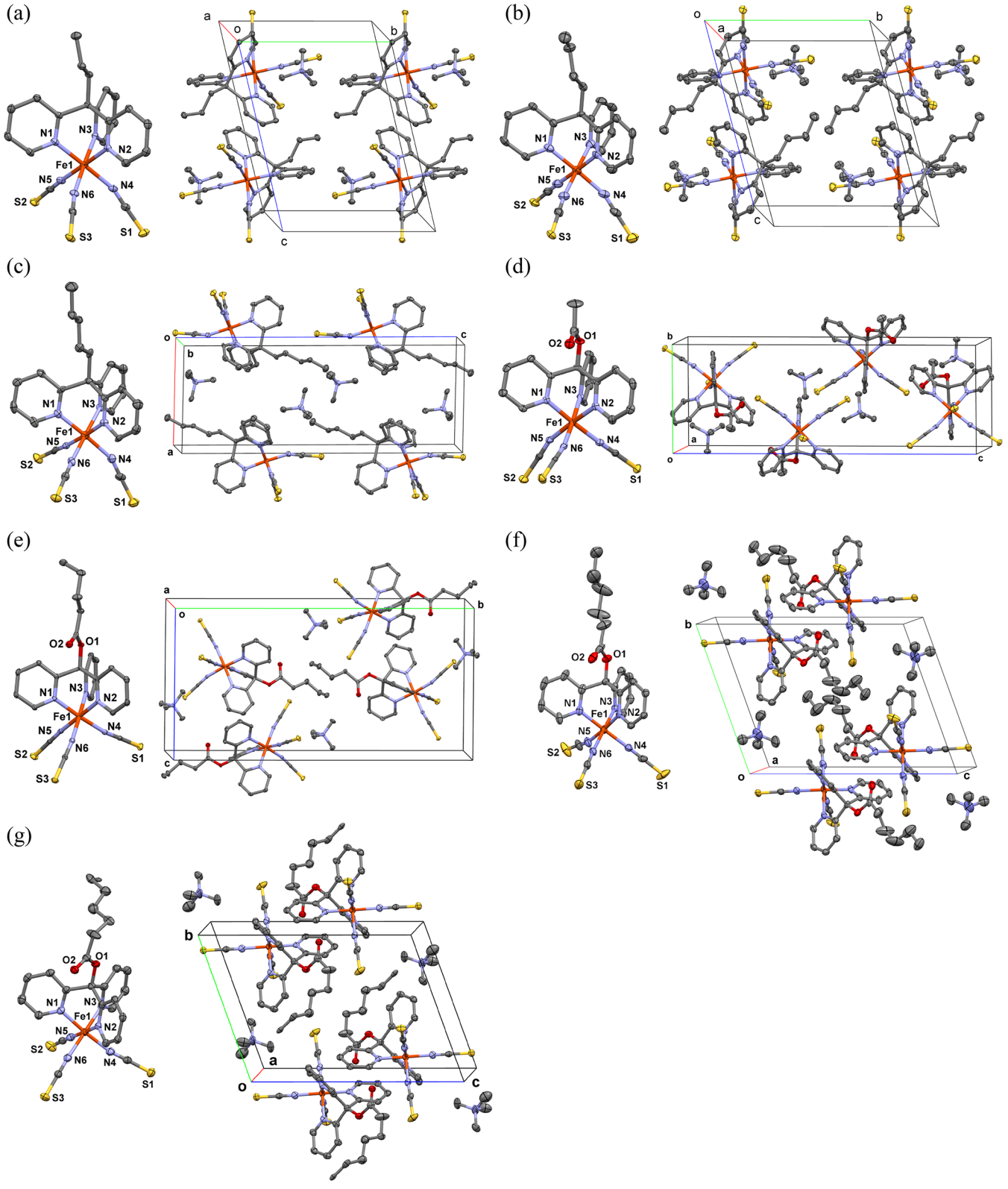


**Figure 1.** Molecular structures of complex anion moieties (left) and packing motifs (right) for (a) **3a**, (b) **4a**, (c) **5a**, (d) **1e**, (e) **4e**, (f) **5e**, and (g) **6e** measured at 100 K. Selected atomic numbering is also shown. Hydrogen atoms are omitted. Thermal ellipsoids are drawn at the 50% probability level. Only a major conformation is drawn for tetramethylammonium cation moieties in (f) and for tetramethylammonium cation and hexyl chain moieties in (g).

in a hexyl chain. The cell constants of **6e** are very close to those of **5e** in the same space group. Actually the total ionic lattices are practically isomorphous. However, the alkyl conformations are different. The pentyl group of **5e** is bent in the *c* axis direction (Figure 1f as a projection view on the *bc* plane), whereas the hexyl group of **6e** in the *b* + *c* direction (Figure


https://dx.doi.org/10.1021/acs.inorgchem.0c01296
*Inorg. Chem.* XXXX, XXX, XXX−XXX

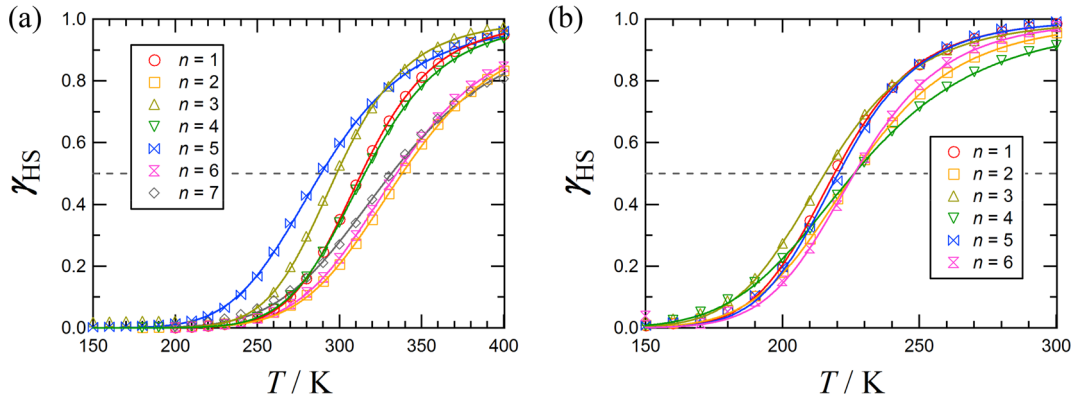


**Figure 2.** Temperature dependence of $\gamma_{HS}$ for (a) **1a**−**7a** and (b) **1e**−**6e**. The solid lines stand for the best fit to the van't Hoff equation. For the parameters, see Table 2.

**Table 2. Optimized Thermodynamic Parameters for 1a−7a and 1e−6e**

| compound | $n$ | $C_0$[a]/cm$^3$ K mol$^{-1}$ | $C_1$/cm$^3$ K mol$^{-1}$ | $T_{1/2}$/K | $\Delta H$/kJ mol$^{-1}$ | $\Delta S$/J K$^{-1}$ mol$^{-1}$ |
|---|---|---|---|---|---|---|
| **1a** | 1 | 3.218(14) | 0.075(4) | 313.4(2) | 36.0(3) | 115(1) |
| **2a** | 2 | 2.35(6) | 0.219(8) | 338.2(15) | 29.8(9) | 88(3) |
| **3a** | 3 | 2.80(7) | 0.00(2) | 298.4(11) | 34.0(16) | 114(5) |
| **4a** | 4 | 3.068(9) | 0.043(2) | 315.4(1) | 33.85(17) | 107(1) |
| **5a** | 5 | 3.27(4) | 0.131(11) | 288.9(6) | 24.4(5) | 84(2) |
| **6a** | 6 | 2.67(2) | 0.068(3) | 334.8(5) | 29.6(3) | 89(1) |
| **7a** | 7 | 2.83(7) | 0.268(10) | 331.7(18) | 24.8(8) | 75(2) |
| **1e** | 1 | 2.84(2) | 0.131(9) | 219.0(2) | 26.2(5) | 120(2) |
| **2e** | 2 | 3.08(5) | 0.20(2) | 226.2(4) | 22.3(6) | 98(3) |
| **3e** | 3 | 3.43(4) | 0.081(13) | 215.6(3) | 22.5(5) | 104(2) |
| **4e** | 4 | 3.84(7) | 0.12(2) | 226.2(5) | 17.9(5) | 79(2) |
| **5e** | 5 | 3.56(6) | 0.02(2) | 220.5(5) | 26.9(10) | 122(4) |
| **6e** | 6 | 3.49(6) | 0.03(2) | 226.3(4) | 25.6(8) | 113(4) |

[a]A $\chi_m T$ contribution proportional to $T$ in the LS phase was subtracted, leading to a small $C_0$ value.

1g). A disorder was found in $Me_4N$ ion as well, and accordingly a loose packing motif is located in a layer parallel to the crystallographic $b + c$ direction.

At this stage, isomorphism has barely been observed among the compounds investigated here, or even we could hardly find out any particular intermolecular interaction in these families. Isomorphous molecular arrangement and alkyl folding motif were characterized only between **3a** and **4a**. The common feature observed here is an approximate bilayer structure. The hydrophobic alkyl groups are located in the clearance of the ionic lattice composed by $Fe(NCS)_3^-$ and $Me_4N^+$ portions. Such a structure has been clarified typically on the stearyl analogue, in which the hydrophobic interaction is definitive in the completely parallel alignment of the stearyl groups,[18e] often referred as a molecular fastener.[24] In sharp contrast to the stearyl case, there is no evidence of parallel or antiparallel aggregation of the alkyl groups in the present series. Even though the shorter alkyl analogues in the present study displayed hydrophobic interaction, the layer character seems to be somewhat vague.

The present complex salts comprise a very large ionic head $(Me_4N)[(SCN)_3Fe(py_3C)$-] and a relatively small alkyl tail ($C_nH_{2n+1}$- and $C_nH_{2n+1}CO_2$-). This structural feature may bring about an incommensurate lattice and void space around the tail, being favorable to the internal motional freedom of the alkyl group.

The crystal structure analysis at 296 K was also carried out on **1e**, **4e**, **5e**, and **6e** (Table S1 and Figure S1, Supporting Information). The crystal system and space group were never changed in comparison with those of 100 K. However, the Fe−N bond lengths at 296 K (2.07−2.24 Å) became ca. 10% longer than those of 100 K. This finding implies that the iron(II) ions are HS and entirely agrees well with the magnetic study (see below); the SCOs of **1e**, **4e**, **5e**, and **6e** were almost completed at 296 K.

**Magnetic Properties.** The magnetic susceptibilities were measured on a SQUID magnetometer, and all of the samples investigated here displayed clear SCO. The raw data are shown in Figures S2 and S3 (Supporting Information). The $\chi_m T$ values in low- and high-temperature sides are consistent with the $S = 0$ and 2 states, respectively.

The SCO profiles were gradual, so that the magnetic data were found to obey the van't Hoff formula (eq 1)[25] on the basis of spin equilibrium, assuming that any rigid crystal effect and cooperativity are minor. The $\chi_m T$ vs $T$ profile was converted to $\gamma_{HS}$ vs $T$ with eq 2, where $\gamma_{HS}$ implies the molar fraction of the HS molecules. Figures 2a and b show the reduced $\gamma_{HS}$ vs $T$ plots for the alkyl and acyloxyl series, respectively. The Curie constant ($C_0$) and an impurity bias ($C_1$) were optimized with numerical analysis (Table 2). Eventually, satisfactory simulated curves are drawn.

$$\gamma_{HS} = \frac{1}{1 + \exp[(\Delta H/R)(1/T - 1/T_{1/2})]} \quad (1)$$

$$\chi_m T = C_0 \gamma_{HS} + C_1 \quad (2)$$


https://dx.doi.org/10.1021/acs.inorgchem.0c01296
Inorg. Chem. XXXX, XXX, XXX−XXX

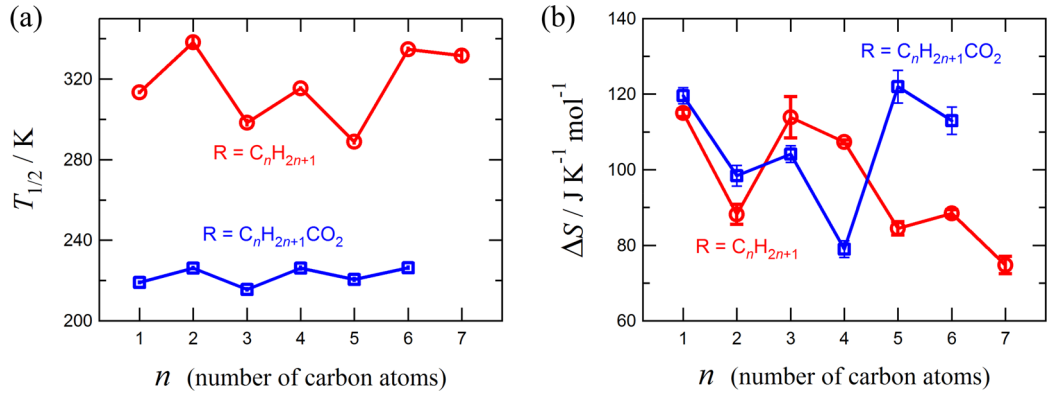


**Figure 3.** (a) SCO temperatures ($T_{1/2}$) of **1a**−**7a** and **1e**−**6e** as a function of the number of carbon atoms in the alkyl side chain ($n$). (b) The molar entropy changes across the SCO ($\Delta S$) in **1a**−**7a** and **1e**−**6e** as a function of $n$.

The SCO temperature $T_{1/2}$ is defined as the temperature at which molar fractions of the HS and LS species are equal. The transition entropy change is related with $\Delta S = \Delta H/T_{1/2}$ because $\Delta G$ vanishes at equilibrium. The thermodynamic parameters $\Delta H$ and $\Delta S$ are also summarized in Table 2.

The $T_{1/2}$ values of the alkyl and acyloxyl families varied in 289−338 K and 216−226 K, respectively (Figure 3a). Note that all the data points are plotted together with an error bar, and the error seems to be considerably reduced, thanks to many data points from the entire temperature range used in the present analysis. The plots of $T_{1/2}$ against $n$ display an up−down alternation, like the melting point of alkanoic acids. The SCO temperatures of the alkyl homologues (**1a**−**7a**) with even $n$ are relatively higher than those of the subset of odd $n$ (a red line in Figure 3a). The $T_{1/2}$ shift is notable as indicated with $\Delta T_{1/2}$ = ca. 30 K. Though the range of the SCO temperatures of the acyloxyl homologues (**1e**−**6e**) is relatively narrow ($\Delta T_{1/2}$ = ca. 10 K), a similar trend is recorded (a blue line in Figure 3a). The acyloxyl family has an additional ester group in between, and it is acceptable that the odd−even effect would be weakened in comparison with that of the alkyl homologues. Actually, as preliminary results, the alkyl homologues with $n \geq 8$ or the acyloxyl homologues with $n \geq 7$ did not show an odd−even effect any more. This effect is found to be remarkable in a range of the short alkyl and acyloxyl chains.

Since the alkyl groups were hardly gathered together in the crystal lattice, the hydrophobic interaction seems to play a minor role in crystallization. This situation is completely different from the known SCO compounds accompanied by supramolecular arrangement of alkyl groups.[6,26,27] In spite of the various packing motifs and intermolecular interactions found among the present compounds, the SCO characteristics unexpectedly displayed a regular up−down alternation profile.

## DISCUSSION

The SCO phenomenon are well-known to have much relation with the crystal field of the iron(II) center.[1] In fact, the suppression of the $T_{1/2}$ of the acyloxylated family, compared to that of the alkylated family, can be explained in terms of the inductive substituent effect from the electronegative oxygen atoms. An octahedral crystal field is weaker, and the HS state is more stabilized, leading to a lower $T_{1/2}$. However, in the present study, attention must be paid to an $n$-dependence on $T_{1/2}$ recorded within each family. It is unlikely that the steric effect from the aliphatic portion modulates the crystal field strength, because of a long distance between the SCO chromophore and terminal alkyl group. It is less likely either that intermolecular interaction regulates the SCO, because the regular up−down alternation appeared, regardless of the various intermolecular contacts.

In theory[28] the entropy difference of SCO can be calculated as a sum of contributions of electronic, vibrational, conformational, rotational, and translational terms (eq 3). In the solid state, two last terms are excluded. The electronic contribution is given with the degeneracy of each state as shown in eq 4. In the case where singlet and quintet states are involved, the electronic contribution is given as $R \ln 5 = 13.38$ J K$^{-1}$ mol$^{-1}$. Strictly speaking, the $\Delta S_{elec}$ term also contains the orbital degeneracy contribution. Obviously, the real geometry of the complex makes this contribution equal to zero.

$$\Delta S = \Delta S_{elec} + \Delta S_{conf} + \Delta S_{vib} + \Delta S_{rot} + \Delta S_{trans} \quad (3)$$

$$\Delta S_{elec} = R \ln \frac{2S_{HS} + 1}{2S_{LS} + 1} \quad (4)$$

Although the SCO temperature ranges are quite different between the two series, the $\Delta S$ values fell in the same range as 75(2)−122(4) J K$^{-1}$ mol$^{-1}$ (Figure 3b). It seems to be helpful to compare with the value $\Delta S$ = 62(1) J K$^{-1}$ mol$^{-1}$ known for R = $C_{18}H_{37}$.[18e,29] In that case, the conformational isomerism has been fully characterized to be an order−disorder-type with respect solely to one C−C bond. Under such conditions, $\Delta S_{conf}$ should be applied as $R \ln 2 = 5.76$ J K$^{-1}$ mol$^{-1}$. Even taking $\Delta S_{conf}$ into account, we find that the residual $\Delta S$ still remains large. It is acceptable that the vibrational contribution around the $FeN_6$ structures would be close to each other in the homologues $Me_4N[Fe(py_3CR)(NCS)_3]$. Accordingly, the $\Delta S_{conf}$ and $\Delta S_{vib}$ contributions would be significant, regarding the degree of freedom due to morphology especially in the alkyl portions.

The excess $\Delta S$ values might be attributed to $\Delta S_{vib}$ and related $\Delta S_{conf}$ contributions. The present compounds have a much shorter alkyl group than $C_{18}H_{37}$, but very interestingly the observed overall entropy changes are comparably larger. It can be pointed out that that the $C_{18}H_{37}$ chain displayed regular trans zigzag conformation for the most part,[18e] possibly thanks to a fastener effect. In other words, the chain seems to be rigid though long. The degree of vibrational freedom in alkyl groups has been considered in relation to isomerism between anti and gauche conformers.[30] This mechanism has been spectroscopically proven in the first-order phase transition observed for ionic conductors based on quaternized 1,4-diazabicyclo[2.2.2]-


https://dx.doi.org/10.1021/acs.inorgchem.0c01296
Inorg. Chem. XXXX, XXX, XXX−XXX

octanes.[31] They exhibited the odd−even effect, which was analyzed in connection with infrared vibration spectroscopy. In the present study, a gauche conformation with appreciable thermal displacement was actually found in **4e**, **5e**, and **6e**. From the large thermal ellipsoids around the gauche-related carbon atoms (Figures 1f and 1g), conformational motions like a crankshaft or a bicycle pedal is possibly assumed. Such an increase of intramolecular motional freedom seems to affect the entropy change in the SCO transformation.

We suppose that the odd−even effect observed here would be ascribable to the intramolecular origin and that the internal conformational motion of the alkyl group seems to be essential. The role of the alkyl groups may reside in regulating the thermodynamic parameters on the basis of the entropy-driven SCO mechanism.

As Figure 3b shows, the entropy changes of **1e**−**6e** showed a regularly alternating dependence. On the other hand, the up−down alternation is violated across **4a**. A similar broken profile has been reported on the odd−even effect in the melting point of linear alkanols, but no structural information has been reported.[32] The finding in the present study is probably related to the difference of the crystal packing motifs ($P\bar{1}$ and $P2_1/c$ for **3a** and **5a**, respectively).

## CONCLUSION

The short linear alkyl and acyloxyl derivatives of $Me_4N[Fe(py_3CR)(NCS)_3]$ with R = $C_nH_{2n+1}$ ($n$ = 1−7) and $C_nH_{2n+1}CO_2$ ($n$ = 1−6) underwent gradual SCO. The plots on $T_{1/2}$ against $n$ displayed the distinct odd−even effect. From the crystallographic study there is no evidence of parallel or antiparallel aggregation of the alkyl groups often referred to as a molecular fastener effect. Instead, there are often found gauche conformations with a severe disorder and thermal displacement in the alkyl chain. The odd−even effect on $T_{1/2}$ may be related with the entropy difference across the SCO, rather than crystal field modification or intermolecular interaction.

The SCO temperatures are located near room temperature, for the alkylated derivatives in particular, being suitable for future application. The $T_{1/2}$ shift is substantial, as large as ca. 30 and 10 K for the alkyl and acyloxyl families, respectively. The present work will help molecular design to fine-tune $T_{1/2}$ by means of simple chemical modification like alkylation and acyloxylation.

## ASSOCIATED CONTENT

### Supporting Information

The Supporting Information is available free of charge at https://pubs.acs.org/doi/10.1021/acs.inorgchem.0c01296.

Table S1, selected crystallographic parameters of **1e**, **4e**, **5e**, and **6e** at 296 K; Figure S1, X-ray crystal structures of **1e**, **4e**, **5e**, and **6e** at 296 K; Figure S2, temperature dependence of product $\chi_m T$ for **1a**−**7a**; Figure S3, temperature dependence of product $\chi_m T$ for **1e**−**6e**; and detailed experimental section (PDF)

### Accession Codes

CCDC 1993173−1993179, 1999658, and 2006066−2006068 contain the supplementary crystallographic data for this paper. These data can be obtained free of charge via www.ccdc.cam.ac.uk/data_request/cif, or by emailing data_request@ccdc.cam.ac.uk, or by contacting The Cambridge Crystallographic Data Centre, 12 Union Road, Cambridge CB2 1EZ, UK; fax: +44 1223 336033.

## AUTHOR INFORMATION


### Corresponding Author

**Takayuki Ishida** − *Department of Engineering Science, The University of Electro-Communications, Chofu, Tokyo 182-8585, Japan*; orcid.org/0000-0001-9088-2526; Email: takayuki.ishida@uec.ac.jp

### Authors

**Atsushi Kashiro** − *Department of Engineering Science, The University of Electro-Communications, Chofu, Tokyo 182-8585, Japan*

**Wakana Kohno** − *Department of Engineering Science, The University of Electro-Communications, Chofu, Tokyo 182-8585, Japan*

Complete contact information is available at: https://pubs.acs.org/10.1021/acs.inorgchem.0c01296


### Notes

The authors declare no competing financial interest.

## ACKNOWLEDGMENTS

This work was financially supported with Izumi Science and Technology Foundation (Grant number 2019-J-033).

## REFERENCES


(1) (a) *Spin Crossover in Transition Metal Compounds I, II, and III*; Gütlich, P., Goodwin, H. A., Eds.; Springer-Verlag: Berlin, Germany, 2004. (b) Molnár, G.; Rat, S.; Salmon, L.; Nicolazzi, W.; Bousseksou, A. Spin Crossover Nanomaterials: From Fundamental Concepts to Devices. *Adv. Mater.* **2018**, *30*, 1703862. (c) Coronado, E. Molecular magnetism: from chemical design to spin control in molecules, materials and devices. *Nature Rev. Mater.* **2020**, *5*, 87−104. (d) *Spin-Crossover Materials: Properties and Applications*; Halcrow, M. A., Ed.; John Wiley & Sons, Inc.: Oxford, UK, 2013; DOI: 10.1002/9781118519301. (e) Halcrow, M. A. Spin-crossover compounds with wide thermal hysteresis. *Chem. Lett.* **2014**, *43*, 1178−1188. (f) Olguin, J. Unusual metal centres/coordination spheres in spin crossover compounds. *Coord. Chem. Rev.* **2020**, *407*, 213148.

(2) (a) Kitazawa, T. Special Issue "Synthesis and Applications of New Spin Crossover Compounds". *Crystals* **2019**, *9*, 382. (b) Takahashi, K. Special Issue "Spin-Crossover Complexes". *Inorganics* **2018**, *6*, 32. (c) Aromí, G.; Real, J. A. Special Issue "Spin Crossover (SCO) Research". *Magnetochem.* **2016**, *2*, 28. (d) Hayami, S.; Holmes, S. M.; Halcrow, M. A. Themed Issue "Spin-State Switches in Molecular Materials Chemistry". *J. Mater. Chem. C* **2015**, *3*, 7775−7978.

(3) (a) Weselski, M. D.; Książek, M.; Mess, P.; Kusz, J.; Bronisz, R. "Normal" and "reverse" spin crossover induced by two different structural events in iron(II) coordination polymer. *Chem. Commun.* **2019**, *55*, 7033−7036. (b) Halcrow, M. A.; Berdiell, I. C.; Pask, C. M.; Kulmaczewski, R. Relationship between the Molecular Structure and Switching Temperature in a Library of Spin-Crossover Molecular Materials. *Inorg. Chem.* **2019**, *58*, 9811−9821. (c) Hogue, R. W.; Singh, S.; Brooker, S. Spin crossover in discrete polynuclear iron(II) complexes. *Chem. Soc. Rev.* **2018**, *47*, 7303−7338.

(4) (a) Létard, J. F.; Guionneau, P.; Nguyen, O.; Costa, J. S.; Marcen, S.; Chastanet, G.; Marchivie, M.; Goux-Capes, L. A Guideline to the Design of Molecular-Based Materials with Long-Lived Photomagnetic Lifetimes. *Chem. - Eur. J.* **2005**, *11*, 4582−4589. (b) Murphy, M. J.; Zenere, K. A.; Ragon, F.; Southon, P. D.; Kepert, C. J.; Neville, S. M. Guest Programmable Multistep Spin Crossover in a Porous 2-D Hofmann-Type Material. *J. Am. Chem. Soc.* **2017**, *139*, 1330−1335.

(5) (a) Kershaw Cook, L. J.; Kulmaczewski, R.; Mohammed, R.; Dudley, S.; Barrett, S. A.; Little, M. A.; Deeth, R. J.; Halcrow, M. A. A Unified Treatment of the Relationship Between Ligand Substituents and Spin State in a Family of Iron(II) Complexes. *Angew. Chem., Int. Ed.* **2016**, *55*, 4327−4331. (b) Kimura, A.; Ishida, T. Spin-Crossover Temperature Predictable from DFT Calculation for Iron(II) Complexes with 4-Substituted Pybox and Related Heteroaromatic Ligands. *ACS Omega* **2018**, *3*, 6737−6747.

(6) Hayami, S.; Komatsu, Y.; Shimizu, T.; Kamihata, H.; Lee, Y. H. Spin-crossover in cobalt(II) compounds containing terpyridine and its derivatives. *Coord. Chem. Rev.* **2011**, *255*, 1981−1990.

(7) (a) Zhang, W.; Zhao, F.; Liu, T.; Yuan, M.; Wang, Z. M.; Gao, S. Spin crossover in a series of iron(II) complexes of 2-(2-alkyl-2*H*-tetrazol-5-yl)-1,10-phenanthroline: Effects of alkyl side chain, solvent, and anion. *Inorg. Chem.* **2007**, *46*, 2541−2555. (b) Galadzhun, I.; Kulmaczewski, R.; Cespedes, O.; Yamada, M.; Yoshinari, N.; Konno, T.; Halcrow, M. A. 2,6-Bis(pyrazol-1-yl)pyridine-4-carboxylate Esters with Alkyl Chain Substituents and Their Iron(II) Complexes. *Inorg. Chem.* **2018**, *57*, 13761−13771. (c) Rosario-Amorin, D.; Dechambenoit, P.; Bentaleb, A.; Rouzieres, M.; Mathoniere, C.; Clerac, R. Multistability at room temperature in a bent-shaped spin-crossover complex decorated with long alkyl chains. *J. Am. Chem. Soc.* **2018**, *140*, 98−101. (d) Weihermüller, J.; Schlamp, S.; Milius, W.; Puchtler, F.; Breu, J.; Ramming, P.; Hüttner, S.; Agarwal, S.; Göbel, C.; Hund, M.; Papastavrou, G.; Weber, B. Amphiphilic iron(II) spin crossover coordination polymers: Crystal structures and phase transition properties. *J. Mater. Chem. C* **2019**, *7*, 1151−1163. (e) Valverde-Muñoz, F. J.; Seredyuk, M.; Meneses-Sanchez, M.; Munoz, M. C.; Bartual-Murgui, C.; Real, J. A. Discrimination between two memory channels by molecular alloying in a doubly bistable spin crossover material. *Chem. Sci.* **2019**, *10*, 3807−3816. (f) Delgado, T.; Tissot, A.; Guenee, L.; Hauser, A.; Valverde-Munoz, F. J.; Seredyuk, M.; Real, J. A.; Pillet, S.; Bendeif, W.-E. Very Long-Lived Photogenerated High-Spin Phase of a Multistable Spin-Crossover Molecular Material. *J. Am. Chem. Soc.* **2018**, *140*, 12870−12876. (g) Weihermüller, J.; Schlamp, S.; Dittrich, B.; Weber, B. Kinetic Trapping Effects in Amphiphilic Iron(II) Spin Crossover Compounds. *Inorg. Chem.* **2019**, *58*, 1278−1289.

(8) (a) Oso, Y.; Ishida, T. Spin-crossover Transition in a Mesophase Iron(II) Thiocyanate Complex Chelated with 4-Hexadecyl-*N*-(2-pyridylmethylene)aniline. *Chem. Lett.* **2009**, *38*, 604−605. (b) Oso, Y.; Kanatsuki, D.; Saito, S.; Nogami, T.; Ishida, T. Spin-crossover Transition Coupled with Another Solid-Solid Phase Transition for Iron(II) Thiocyanate Complexes Chelated with Alkylated *N*-(Di-2-pyridylmethylene)anilines. *Chem. Lett.* **2008**, *37*, 760−761.

(9) (a) Galyametdinov, Y.; Ksenofontov, V.; Prosvirin, A.; Ovchinnikov, I.; Ivanova, G.; Gutlich, P.; Haase, W. First Example of Coexistence of Thermal Spin Transition and Liquid-Crystal Properties. *Angew. Chem., Int. Ed.* **2001**, *40*, 4269−4271. (b) Gaspar, A. B.; Seredyuk, M. Spin crossover in soft matter. *Coord. Chem. Rev.* **2014**, *268*, 41−58. (c) Akiyoshi, R.; Hirota, Y.; Kosumi, D.; Tsutsumi, M.; Nakamura, M.; Lindoy, L. F.; Hayami, S. Ferroelectric metallomesogens composed of achiral spin crossover molecules. *Chem. Sci.* **2019**, *10*, 5843−5848. (d) Rocha, M. A. A.; Coutinho, J. A. P.; Santos, L. M. N. B. F. Vapor pressures of 1,3-dialkylimidazolium bis(trifluoromethylsulfonyl)imide ionic liquids with long alkyl chains. *J. Chem. Phys.* **2014**, *141*, 134502. (e) de la Rama, L. P.; Hu, L.; Efremov, M. Y.; Allen, L. H. Size Effect and Odd-Even Alternation in the Melting of Single and Stacked AgSC*n* Layers: Synthesis and Nanocalorimetry Measurements. *J. Am. Chem. Soc.* **2013**, *135*, 14286−14298. (f) Romero-Morcillo, T.; Seredyuk, M.; Munoz, M. C.; Real, J. A. Meltable Spin Transition Molecular Materials with Tunable $T_c$ and Hysteresis Loop Width. *Angew. Chem., Int. Ed.* **2015**, *54*, 14777−14781.

(10) (a) Knothe, G.; Dunn, R. O. A Comprehensive Evaluation of the Melting Points of Fatty Acids and Esters Determined by Differential Scanning Calorimetry. *J. Am. Oil Chem. Soc.* **2009**, *86*, 843−856. (b) Mishra, M. K.; Varughese, S.; Ramamurty, U.; Desiraju, G. R. Odd-Even Effect in the Elastic Modulii of α,ω-Alkanedicarboxylic Acids. *J. Am. Chem. Soc.* **2013**, *135*, 8121−8124.

(11) (a) Joseph, S.; Sathiskumar, R. Succinate esters: odd−even effects in melting points. *Acta Crystallogr., Sect. B: Struct. Sci., Cryst. Eng. Mater.* **2014**, *70*, 839−846. (b) Aparicio, F.; Matesanz, E.; Sanchez, L. Breaking the Odd-Even Effect in the Self-Assembly of Linear Bis(benzamides). *Chem. - Eur. J.* **2014**, *20*, 14599−14603.

(12) (a) Prabhu, R.; Yelamaggad, C. V. Structure-Property Correlations in Cyanobiphenyl-Based Dimer-Like Mesogens. *J. Phys. Chem. B* **2015**, *119*, 11935−11952. (b) Usuda, H.; Hishida, M.; Yamamura, Y.; Saito, K. Contrasting Effects of a Rigid Core and an Alkyl Chain in nCB on the Phase Behavior of Lipid Bilayers. *Langmuir* **2016**, *32*, 5966−5972.

(13) (a) Kitamura, C.; Abe, Y.; Ohara, T.; Yoneda, A.; Kawase, T.; Kobayashi, T.; Naito, H.; Komatsu, T. Synthesis and Crystallochromy of 1,4,7,10-Tetraalkyltetracenes: Tuning of Solid-State Optical Properties of Tetracenes by Alkyl Side-Chain Length. *Chem. - Eur. J.* **2010**, *16*, 890−898. (b) Anuradha; Al Kobaisi, M.; Gupta, A.; Bhosale, S. V.; La, D. D. Chiral Assembly of AIE-Active Achiral Molecules: An Odd Effect in Self-Assembly. *Chem. - Eur. J.* **2017**, *23*, 3950−3956.

(14) (a) Kim, K.; Plass, K. E.; Matzger, A. J. Structure of and Competitive Adsorption in Alkyl Dicarbamate Two-Dimensional Crystals. *J. Am. Chem. Soc.* **2005**, *127*, 4879−4887. (b) Mochizuki, E.; Yasui, N.; Kai, Y.; Inaki, Y.; Yuhua, W.; Saito, T.; Tohnai, N.; Miyata, M. Crystal Structure of Long Alkyl 3-(Thymin-1-yl)propionates: Style of Hydrogen Bonding and Dependence on the Alkyl Chain Length. *Bull. Chem. Soc. Jpn.* **2001**, *74*, 193−200.

(15) (a) Tao, F.; Bernasek, S. L. Understanding Odd-Even Effects in Organic Self-Assembled Monolayers. *Chem. Rev.* **2007**, *107*, 1408−1453. (b) Yu, H.; Park, K. H.; Song, I.; Kim, M.-J.; Kim, Y.-H.; Oh, J. H. Effect of the alkyl spacer length on the electrical performance of diketopyrrolopyrrole-thiophene vinylene thiophene polymer semiconductors. *J. Mater. Chem. C* **2015**, *3*, 11697−11704. (c) Feng, Y.; Dionne, E. R.; Toader, V.; Beaudoin, G.; Badia, A. Odd-Even Effects in Electroactive Self-Assembled Monolayers Investigated by Electrochemical Surface Plasmon Resonance and Impedance Spectroscopy. *J. Phys. Chem. C* **2017**, *121*, 24626−24640. (d) Dendzik, M.; Terfort, A.; Cyganik, P. Odd-Even Effect in the Polymorphism of Self-Assembled Monolayers of Biphenyl-Substituted Alkaneselenolates on Au(111). *J. Phys. Chem. C* **2012**, *116*, 19535−19542.

(16) Burrows, H. D. Studying Odd-Even Effects and Solubility Behavior Using α,ω-Dicarboxylic Acids. *J. Chem. Educ.* **1992**, *69*, 69−72.

(17) Sivaramakrishna, D.; Swamy, M. J. Self-Assembly, Supramolecular Organization, and Phase Behavior of L-Alanine Alkyl Esters ($n$ = 9−18) and Characterization of Equimolar L-Alanine Lauryl Ester/Lauryl Sulfate Catanionic Complex. *Langmuir* **2015**, *31*, 9546−9556.

(18) (a) Yamasaki, M. T.; Ishida, T. Heating-rate dependence of spin-crossover hysteresis observed in an iron(II) complex having tris(2-pyridyl)methanol. *J. Mater. Chem. C* **2015**, *3*, 7784−7787. (b) Ishida, T.; Kanetomo, T.; Yamasaki, M. An iron(II) complex tripodally chelated with 1,1,1-tris-(pyridin-2-yl)ethane showing room-temperature spin-crossover behaviour. *Acta Crystallogr., Sect. C: Struct. Chem.* **2016**, *72*, 797−801. (c) Yamasaki, M.; Ishida, T. Spin-crossover thermal hysteresis and light-induced effect on iron(II) complexes with tripodal tris(2-pyridyl)methanol. *Polyhedron* **2015**, *85*, 795−799. (d) Hirosawa, N.; Oso, Y.; Ishida, T. Spin Crossover and Light-induced Excited Spin-state Trapping Observed for an Iron(II) Complex Chelated with Tripodal Tetrakis(2-pyridyl)methane. *Chem. Lett.* **2012**, *41*, 716−718. (e) Kashiro, A.; Some, K.; Kobayashi, Y.; Ishida, T. Iron(II) and 1,1,1-Tris(2-pyridyl)nonadecane Complex Showing an Order-Disorder-Type Structural Transition and Spin-Crossover Synchronized over Both Conformers. *Inorg. Chem.* **2019**, *58*, 7672−7676. (f) Yamasaki, M.; Ishida, T. First Iron(II) Spin-crossover Complex with an $N_5S$ Coordination Sphere. *Chem. Lett.* **2015**, *44*, 920−921.


https://dx.doi.org/10.1021/acs.inorgchem.0c01296
*Inorg. Chem.* XXXX, XXX, XXX−XXX

(19) (a) Nebbali, K.; Mekuimemba, C. D.; Charles, C.; Yefsah, S.; Chastanet, G.; Mota, A. J.; Colacio, E.; Triki, S. One-Dimensional Thiocyanato-Bridged Fe(II) Spin Crossover Cooperative Polymer With Unusual $FeN_5S$ Coordination Sphere. *Inorg. Chem.* **2018**, *57*, 12338−12346. (b) Mekuimemba, C. D.; Conan, F.; Mota, A. J.; Palacios, M. A.; Colacio, E.; Triki, S. On the Magnetic Coupling and Spin Crossover Behavior in Complexes Containing the Head-to-Tail $[Fe^{II}_2(\mu\text{-SCN})_2]$ Bridging Unit: A Magnetostructural Experimental and Theoretical Study. *Inorg. Chem.* **2018**, *57*, 2184−2192.
(20) (a) Maleckis, A.; Kampf, J. W.; Sanford, M. S. A Detailed Study of Acetate-Assisted C-H Activation at Palladium(IV) Centers. *J. Am. Chem. Soc.* **2013**, *135*, 6618−6625. (b) Ünal, E. A.; Wiedemann, D.; Seiffert, J.; Boyd, J. P.; Grohmann, A. Efficient synthesis of pentakis- and tris(pyridine) ligands. *Tetrahedron Lett.* **2012**, *53*, 54−55.
(21) White, D. L.; Faller, J. W. Preparation and reactions of the $C_{3v}$ ligand tris(2-pyridyl)methane and its derivatives. *Inorg. Chem.* **1982**, *21*, 3119−3122.
(22) Guionneau, P.; Marchivie, M.; Bravic, G.; Letard, J.-F.; Chasseau, D. Structural Aspects of Spin Crossover. Example of the $[Fe^{II}L_n(NCS)_2]$ Complexes. *Top. Curr. Chem.* **2004**, *234*, 97−128.
(23) Bondi, A. van der Waals Volumes and Radii. *J. Phys. Chem.* **1964**, *68*, 441−451.
(24) Imaeda, K.; Enoki, T.; Shi, Z.; Wu, P.; Okada, N.; Yamochi, H.; Saito, G.; Inokuchi, H. Electrical Conductivities of Tetrakis-(alkylthio)tetrathiafulvalene (TTCn-TTF) and Tetrakis(alkyltelluro)-tetrathiafulvalene (TTeCn-TTF). *Bull. Chem. Soc. Jpn.* **1987**, *60*, 3163−3167.
(25) (a) Boca, R., Ed., *Theoretical Foundations of Molecular Magnetism: Current Methods in Inorganic Chemistry*; Elsevier: Amsterdam, 1999; Vol. *1*, pp 541−563. (b) Kahn, O., Ed., *Molecular Magnetism*; VCH: New York, 1993; pp 53−69.
(26) Akiyoshi, R.; Kuroiwa, K.; Amolegbe, S. A.; Nakaya, M.; Ohtani, R.; Nakamura, M.; Lindoy, L. F.; Hayami, S. Supramolecular architectures self-assembled using long chain alkylated spin crossover cobalt(II) compounds. *Chem. Commun.* **2017**, *53*, 4685−4687.
(27) Sugahara, A.; Kamebuchi, H.; Okazawa, A.; Enomoto, M.; Kojima, N. Control of Spin-Crossover Phenomena in One-Dimensional Triazole-Coordinated Iron(II) Complexes by Means of Functional Counter Ions. *Inorganics* **2017**, *5*, 50.
(28) (a) Molnár, G.; Mikolasek, M.; Ridier, K.; Fahs, A.; Nicolazzi, W.; Bousseksou, A. Molecular Spin Crossover Materials: Review of the Lattice Dynamical Properties. *Ann. Phys. (Berlin, Ger.)* **2019**, *531*, 1900076−21. (b) Cirera, J.; Via-Nadal, M.; Ruiz, E. Benchmarking Density Functional Methods for Calculation of State Energies of First Row Spin-Crossover Molecules. *Inorg. Chem.* **2018**, *57*, 14097−14105. (c) Valtiner, M.; Paulsen, H.; Weinberger, P.; Linert, W. Theoretical investigations of a series of [*hexakis*(1-(tetrazol-1-yl)alkane-*N*4)iron(II)] *bis*(tetrafluoroborate) spin crossover complexes: Methyl- to pentyl substituted species in the approximation of free cations. *MATCH Commun. Math. Comput. Chem.* **2007**, *57*, 749−761.
(29) The $C_{18}$ chain has larger entropy due to the greater thermal motion than the short chains have. The present analysis deals with the difference between the entropies in the high- and low-temperature phases, so that the essential entropy due to the $C_{18}$ skeleton is canceled for the most part. Similarly, the most entropies due to the shorter skeletons are canceled. It is the reason that the phase transition entropy changes are comparable among the long- to short-chain derivatives.
(30) McClure, D. W. Nature of the Rotational Phase Transition in Paraffin Crystals. *J. Chem. Phys.* **1968**, *49*, 1830−1839.
(31) (a) Shimizu, J.; Imamura, K.; Nogami, T.; Mikawa, H. Phase Transition of Quaternary Alkyl Halide Salts of 1,4-Diazabicyclo[2.2.2]octane. *Bull. Chem. Soc. Jpn.* **1986**, *59*, 1443−1448. (b) Toyama, Y.; Murakami, K.; Yoshimura, N.; Takayanagi, M. Even-odd alternation of near-infrared spectra of alkane-$\alpha,\omega$-diols in their solid states. *Spectrochim. Acta, Part A* **2018**, *197*, 148−152.
(32) Costa, J. C. S.; Mendes, A.; Santos, L. M. N. B. F. Chain Length Dependence of the Thermodynamic Properties of n-Alkanes and their Monosubstituted Derivatives. *J. Chem. Eng. Data* **2018**, *63*, 1−20.


https://dx.doi.org/10.1021/acs.inorgchem.0c01296
*Inorg. Chem.* XXXX, XXX, XXX−XXX